J. Fluid Mech. (2021), *vol*. 918, A15, doi:10.1017/jfm.2021.328

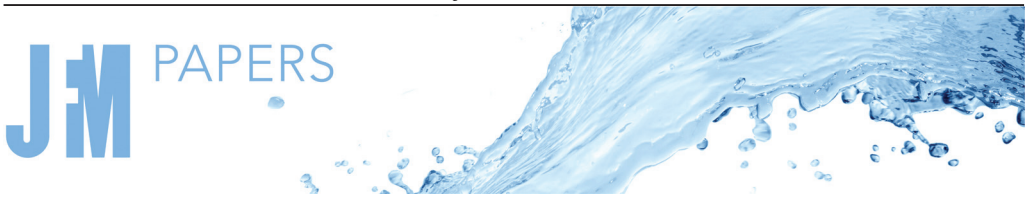

Force on a moving liquid blister

Zhi-Qiao Wang[1] **and Emmanuel Detournay**[2],†

[1]School of Engineering and Technology, China University of Geosciences, Beijing 100083, PR China

[2]Department of Civil, Environmental, and Geo- Engineering, University of Minnesota, Minneapolis, MN 55455, USA

(Received 19 April 2020; revised 10 February 2021; accepted 7 April 2021)

This paper investigates the motion of a liquid blister, trapped between an elastic sheet and a rigid substrate. The blister is driven by a frictionless blade moving at a constant velocity, forcing a constant gap that causes fluid to bleed from the blister. The sheet adheres to the substrate ahead of the blister. The main goal of the study is to assess the magnitude and orientation of the force applied by the blade on the moving blister. The solution is constructed for the asymptotic case of a long blister. Thanks to a separation of scales, the asymptotic solution is obtained by matching the boundary layers at the front end and at the back end of the blister to an outer solution characterised by a uniform pressure in the bulk. Both boundary layers are formulated as travelling-wave equations for the gap between the sheet and the substrate. The formulation accounts for a moving fluid front, distinct from the separation edge, and for a tail with a gap tending to an *a priori* unknown value far behind the blister. Scaling of the governing equations indicates that the solution depends on two numbers: a dimensionless toughness $\mathcal{K}$ and a scaled gap $\mathcal{W}$ imposed by the moving blade. The key result concerns the dependence of the scaled force on the two numbers controlling the solution of the moving liquid blister. There are two asymptotic solutions: for small gaps at the blade, the force on the blade is dominated by viscous dissipation at the back end and only depends on aperture $\mathcal{W}$; for large gaps, the horizontal force H only depends on toughness $\mathcal{K}$, a function of both fluid viscosity and energy of separation at the front end, whereas the vertical force V depends on both $\mathcal{K}$ and $\mathcal{W}$.

Key words: boundary-layer structure, lubrication theory

1. Introduction

Processes involving fluid-driven separation of an elastic sheet from a stiff substrate are ubiquitous in geosciences and engineering. Emplacement of shallow magmatic intrusions

† Email address for correspondence: detou001@umn.edu

© The Author(s), 2021. Published by Cambridge University Press. This is an Open Access article, distributed under the terms of the Creative Commons Attribution licence (http://creativecommons.org/licenses/by/4.0/), which permits unrestricted re-use, distribution, and reproduction in any medium, provided the original work is properly cited.

https://doi.org/10.1017/jfm.2021.328 Published online by Cambridge University Press

(Bunger & Cruden 2011; Michaut 2011; Thorey & Michaut 2016), and the flow-driven formation of a cavity at the contact between an ice sheet and bedrock caused by rapid drainage of supraglacial lakes (Tsai & Rice 2012; Hewitt, Chini & Neufeld 2018) are large-scale instances of such processes in nature. Excavation of hard rocks (Young 1999), cave inducement in mining (Jeffrey *et al.* 2000) and contaminant spill remediation (Murdoch 2002) represent examples of engineered hydraulic fractures near a free surface. Other technological applications include the manufacturing of silicon wafers (Tayler & King 1987; King 1989), the fabrication of micro-electro-mechanical systems (Hosoi & Mahadevan 2004) and the liquid-blister test to measure the adhesive strength of the interface due to the surface tension of an interstitial fluid layer (Chopin, Vella & Boudaoud 2008).

Many of these problems can advantageously be modelled as the peeling, by bending, of an elastic sheet from a rigid adhesive substrate (Flitton & King 2004; Lister, Peng & Neufeld 2013). Models based on beam or plate theory, lubrication theory and fracture mechanics lead to the formulation of a sixth-order nonlinear diffusion equation (Flitton & King 2004; Lister *et al.* 2013; Hewitt, Balmforth & De Bruyn 2015), which governs the evolution of the fluid-filled gap between the elastic sheet and the substrate. However, this equation does not have a solution if the fluid is assumed to fully fill the growing cavity. Indeed the conditions of zero flux and zero aperture at the moving front lead to a singular solution that is not compatible with the underlying hypotheses (Tayler & King 1987; Flitton & King 2004; Lister *et al.* 2013; Hewitt *et al.* 2015).

Different forms of regularisation of the solution in the tip region have been proposed in recent studies. These include assuming the existence of a thin pre-wetting film of fluid of constant thickness (Flitton & King 2004; Lister *et al.* 2013; Hewitt *et al.* 2015); relaxing the impermeability constraint so as to allow leak-off of the injected fluid in the permeable substrate (Hewitt *et al.* 2018); introducing a moving-fluid front that lags behind the separation front (Hewitt *et al.* 2015; Ball & Neufeld 2018; Wang & Detournay 2018); and finally considering the full elasticity equations rather than the simplified Euler–Bernoulli equations governing the bending of the elastic sheet, on account that these latter equations are not applicable within a distance of order of the layer thickness from the tip (Lister, Skinner & Large 2019). As the global solution is critically dependent on the dynamics of the separation front, the form of regularisation has to be motivated by the physics of the problem. For example, it is not realistic to invoke the presence of a pre-wetting film of fluid for a hydraulic fracture propagating along an initially dry adhesive interface.

In this paper we consider the motion of a two-dimensional liquid blister trapped between a rigid substrate and an adhering elastic sheet, with the goal of assessing the force required to displace the blister. The motion of the blister is driven by a frictionless blade that is kinematically constrained to locally impose a constant gap between the sheet and the substrate. The complete closure of this gap to prevent bleeding of the blister at its back end would require the application of an infinite force on the blade, as could be surmised from the related problem of scraping a viscous fluid from a plane surface (Taylor 1962; Giacomin *et al.* 2012; Seiwert, Quéré & Clanet 2013). However, the gap far behind the blister is itself an unknown, not unlike the residual film thickness in the elastic Landau–Levitch dip-coating problem, which involves withdrawal of a plate from a bath of fluid covered by a thin elastic interface (Landau & Levich 1942; Dixit & Homsy 2013; Warburton, Hewitt & Neufeld 2020). A common example of application of this simplified model is the attempted removal of a viscous blister from a wallpaper by sliding a blade on the paper.

The paper is structured as follows. First, the moving blister problem is formulated in terms of the gap between the elastic sheet and the rigid substrate. The formulation accounts

https://doi.org/10.1017/jfm.2021.328 Published online by Cambridge University Press

for a moving fluid front distinct from the separation edge at the front end of the blister and for a tail with a residual gap behind the blister. An asymptotic solution for a long blister is then described. Scaling of the governing equations indicates that this asymptotic solution depends on two numbers: one can be interpreted as a dimensionless toughness, the other is a scaled measure of the gap imposed by the blade. A separation of scales allows for the construction of a solution obtained by matching boundary layers at the front end and at the back end to an outer solution in the bulk of the blister. The key result concerns the dependence of the scaled force on the two numbers controlling the solution of the moving liquid blister.

2. Mathematical description

2.1. *Problem definition*

Figure 1 illustrates a liquid blister forced to advance between a thin elastic sheet and a rigid substrate by the action of a rigid frictionless blade moving at constant velocity v, while enforcing a constant gap w_0 at the blister back end. The elastic layer of thickness h is characterised by flexural rigidity $D = Eh^3/12(1-\nu^2)$, where E is Young's modulus and ν is Poisson's ratio. The fluid is assumed to be incompressible and Newtonian with viscosity μ. Ahead of the blister, the elastic sheet adheres to the substrate. The strength of the interface is characterised by adhesion energy G_c, whose dissipation is assumed to be localised at the separation front. The blister consists of a fluid-filled part and a cavity at the front filled with fluid vapours, which is at negative pressure $-\sigma_0$, with the atmospheric pressure taken as reference. There is therefore a lag between the separation front and the fluid front. A residual fluid film trapped between the sheet and the substrate is left behind the blister. This region, assumed to be infinite, is referred to as the tail.

Although the existence of fluid lag at the front end of the blister is a requirement to avoid a pressure singularity incompatible with the underlying mathematical model, a gap w_0 is required at the receding end of the blister, where the blade touches the elastic sheet, to regularise the pressure singularity that would otherwise arise. Both the fluid lag λ and the residual gap w_∞ far behind the blade are *a priori* unknown and thus part of the solution.

The blister is characterised by three moving boundaries: a separation front where the elastic layer breaks away from the substrate, a fluid front lagging behind the separation front and a receding front at the blade. In the moving coordinate system with origin at the blade, $x = X - vt$, where X is a fixed coordinate and t is time, the separation front is located at $x = \ell(t)$, the fluid front at $x = \ell_f(t)$, with $\ell_f = \ell - \lambda$. The geometry of the blister and of the tail is described by the gap thickness $w(x, t)$, which also represents the deflection of the elastic sheet.

The force $\boldsymbol{F}$ imparted by the frictionless blade pressing down on the sheet to squeeze the fluid forward is normal to the neutral axis of the sheet. As the slope of the elastic sheet at the point of contact is $w'(0, t) > 0$, the horizontal component H of force $\boldsymbol{F}$ can be expressed as $H = Vw'(0, t)$, where V the vertical component given by $V = D(w'''(0^-, t) - w'''(0^+, t))$ within the approximation of Euler–Bernoulli beam theory. When the blister propagates, the external power Hv balances the dissipation at the propagation front, which is associated with the delamination of the sheet from the substrate, the dissipation in the viscous fluid and the rate of change of the elastic energy in the sheet.

In summary, the set of parameters $\mathcal{S}$ defining the moving blister problem consists of the blade velocity v, the imposed gap w_0 at the blade, the adhesion energy G_c, the bending stiffness D, the viscosity μ and the negative lag pressure $-\sigma_0$. Clearly, the problem is time dependent and its solution requires the initial conditions be defined. However, the solution

https://doi.org/10.1017/jfm.2021.328 Published online by Cambridge University Press

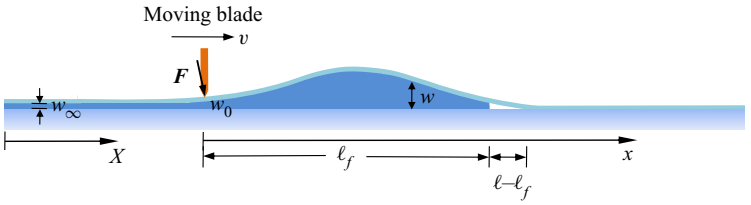

Figure 1. Liquid blister trapped between an elastic sheet and a rigid substrate. The blister is driven by a steadily moving blade, kinematically constrained to enforce a constant gap w_0 at the receding back end of the blister. A negative pressure $-\sigma_0$ acts in the lag cavity behind the separation front.

eventually reaches a quasi-steady state in the limit $w_0 \to 0$, with the volume of fluid in the blister remaining approximately constant.

2.2. *Governing equations*

To complete the description of the problem, we introduce fluid pressure $p(x, t)$ and fluid flux $q(x, t)$ measured relative to the fixed coordinate X. In the lag region $\ell_f < x < \ell$, the vapour pressure is $p = -\sigma_0$, recalling that the atmospheric pressure is taken as reference. The fluid pressure vanishes sufficiently far behind the blade in order to satisfy static equilibrium between the fluid film and the elastic sheet.

The equations governing the unknown fields in both the blister and the tail, as well as the evolution of the blister length ℓ and of the fluid lag $\lambda = \ell - \ell_f$ are formulated in the moving coordinate system attached to the blade. The elastic sheet is viewed as a Euler–Bernoulli beam and thus its deflection $w(x, t)$ is related to the net pressure p according to

$$D\frac{\partial^4 w}{\partial x^4} = p, \quad x \in [-\infty, \ell] \tag{2.1}$$

noting that $p = -\sigma_0$ in the lag region $\ell_f < x \leq \ell$. The flow of fluid in the moving blister is assumed to be governed by lubrication theory. Within this description, the continuity equation written in the moving coordinate system yields

$$\frac{\partial w}{\partial t} - v\frac{\partial w}{\partial x} + \frac{\partial q}{\partial x} = 0, \quad x \in [-\infty, \ell_f] \tag{2.2}$$

and Poiseuille law reads

$$q = -\frac{w^3}{\mu'}\frac{\partial p}{\partial x}, \tag{2.3}$$

where $\mu' = 12\mu$ is introduced to remove numerical factors from the scales defined in § 3.

These three equations together with the initial gap profile and the following conditions on $w(x, t)$ constitute a closed system of equations to determine the blister thickness $w(x, t)$, length $\ell(t)$ and lag $\lambda(t)$ as functions of the parameter set $\mathcal{S}$.

2.2.1. *At the delamination front $x = \ell$*

The geometrical conditions are

$$w = \frac{\partial w}{\partial x} = 0, \tag{2.4}$$

https://doi.org/10.1017/jfm.2021.328 Published online by Cambridge University Press

and the separation criterion is

$$\frac{\partial^2 w}{\partial x^2} = \left(\frac{2G_c}{D}\right)^{1/2}. \tag{2.5}$$

The second condition (2.4) results from the assumption that the substrate is rigid and that the delamination is localised at the moving front. The separation condition (2.5) expresses the curvature at the peeling front in terms of the ratio of the critical energy release rate and the bending stiffness (Landau & Lifshitz 1986; Hutchinson & Suo 1991; Majidi & Adams 2009).

2.2.2. *At the fluid front ($x = \ell_f$)*
The movement of the fluid front is determined by the Stefan condition

$$v + \frac{\mathrm{d}\ell_f}{\mathrm{d}t} = \frac{q}{w}. \tag{2.6}$$

There are five continuity conditions

$$\left[\frac{\partial^i w}{\partial x^i}\right] = 0, \quad i = 0, \ldots, 4, \tag{2.7}$$

where $[f(\ell)] = f(x)|_{x=\ell_f^+} - f(x)|_{x=\ell_f^-}$. In particular, continuity of the fourth-order derivative represents continuity of the pressure at the fluid front, i.e. $p(\ell_f) = -\sigma_0$.

2.2.3. *In the receding region ($x \leq 0$)*
The aperture at the blade is known,

$$w = w_0, \quad x = 0. \tag{2.8}$$

With the net pressure vanishing far behind the blister, the gap tends to a constant but unknown value $w_\infty(t)$,

$$w = w_\infty(t), \quad x \to -\infty. \tag{2.9}$$

Once $w(x, t)$ has been determined by solving the system of (2.4)–(2.8), the components of the force $\boldsymbol{F}$ applied by the blade, normal and parallel to its motion can be deduced from the slope of the deflection and the jump of the shear force at $x = 0$.

2.3. *Long blister limit*

The asymptotic solution for a long blister is characterised by the existence of a central region with a quasi-uniform pressure, to which are appended two boundary layers: one at the front of the blister, the other at the back. The boundary layers can be considered as being quasi-autonomous and can thus be approximated as a travelling wave. However, in the limiting case $w_0 \to 0$, the whole solution is in the form of a travelling wave, after undergoing some transient evolution from an initial state at rest.

This structure of the long-blister asymptotic solution rests on two key points. First, the matched curvature between the front-end boundary layer and the core region is the same as the matched curvature at the back-end boundary layer, a consequence of the front–back symmetry of the outer solution resulting in part from the uniformity of the pressure in the central region. Second, the velocity v' of the separation front and of the fluid front is to first order the same as the velocity v of the blade. Actually, as demonstrated in Appendix A,

https://doi.org/10.1017/jfm.2021.328 Published online by Cambridge University Press

$v' = (1 - \epsilon(t))v$, where $\epsilon \sim w_\infty \ell^{-2}$, noting that $w_\infty \to 0$ and thus $v' \to v$ in the limit $w_0 \to 0$. Thus, although the blister progressively contracts as it is bleeding fluid through the gap at the blade, the solutions in the boundary layers are to first order translationally time invariant.

The outer solution of the central region couples the two boundary layers: the back imposes the front velocity, but the front imposes the matched curvature at the back, which ultimately controls the force on the blade under certain conditions. With the matched curvature remaining constant to first order, the uniform pressure in the core region of the blister varies according to $p \sim \ell^{-2}$ (this dependence of p on the blister length could be translated into a dependence on time t, on account that the bleeding rate is to first order constant in the long-blister asymptotic case).

In the boundary layers, the continuity equation (2.2) can therefore be simplified to

$$v\frac{\mathrm{d}w}{\mathrm{d}x} = \frac{\mathrm{d}q}{\mathrm{d}x}. \tag{2.10}$$

Integrating this equation yields

$$q = vw \tag{2.11}$$

in the front-end boundary layer, but

$$q = v(w - w_\infty) \tag{2.12}$$

in the back-end boundary layer. The difference between these two integrated continuity equations stems from the Stefan condition at the front and the zero flux condition at $x \to -\infty$. Combining the Euler–Bernoulli equation (2.1) with Poiseuille's law (2.3) and either (2.11) or (2.12) yields a fifth-order nonlinear ordinary differential equation (ODE) governing the gap $w(x)$ in the fluid-filled part of the front layer and in the back layer.

3. Scaling

The structure of the asymptotic solution for a long blister, a central region under quasi-uniform pressure, sandwiched between two boundary layers, is confirmed by a scaling analysis, which further shows that the solution in the boundary layers actually depends on two numbers: toughness $\mathcal{K}$ and imposed gap $\mathcal{W}$ at the blade. As the focus of this study is to determine the quasi-stationary force required to drive the blade, we avoid conducting a scaling analysis of the general set of equations by considering the limiting case $w_0 \to 0$, which accepts a travelling-wave solution. The back-end boundary layer in the general case $w_0 > 0$ then naturally depends on the additional number $\mathcal{W}$.

Let ℓ_* and w_* denote scales for the blister length and thickness, respectively. We then define the dimensionless gap Ω, coordinate ξ, fluid front position γ_f and lag Λ

$$\Omega = \frac{w}{\gamma_f^\alpha w_*}, \quad \xi = \frac{x}{\ell_f}, \quad \gamma_f = \frac{\ell_f}{\ell_*}, \quad \Lambda = \frac{\ell - \ell_f}{\ell_*} = \frac{\lambda}{\ell_*}. \tag{3.1a–d}$$

Considering the limiting case $w_0 = 0$, for which the solution is only defined on $x \in [0, \ell]$, and assuming that ℓ_f is used as proxy for the volume of fluid trapped in the blister (because a one-to-one relationship exists between these two parameters), the nonlinear system of

https://doi.org/10.1017/jfm.2021.328 Published online by Cambridge University Press

equations governing $\Omega(\xi)$ at steady state are

$$\Omega^2 \frac{\mathrm{d}^5\Omega}{\mathrm{d}\xi^5} = -\mathcal{G}_m \gamma_f^{5-3\alpha}, \quad \xi \in [0, 1], \tag{3.2}$$

$$\frac{\mathrm{d}^4\Omega}{\mathrm{d}\xi^4} = -\mathcal{G}_s \gamma_f^{4-\alpha}, \quad \xi \in \left[1, 1 + \frac{\Lambda}{\gamma_f}\right], \tag{3.3}$$

$$\Omega = \frac{\mathrm{d}\Omega}{\mathrm{d}\xi} = 0, \quad \frac{\mathrm{d}^2\Omega}{\mathrm{d}\xi^2} = \mathcal{G}_k \gamma_f^{2-\alpha}, \quad \text{at } \xi = 1 + \frac{\Lambda}{\gamma_f}, \tag{3.4a,b}$$

$$\Omega = 0, \quad \text{at } \xi = 0. \tag{3.5}$$

Three dimensionless groups appear in the above equations:

$$\mathcal{G}_m = \frac{\mu' v \ell_*^5}{D w_*^3}, \quad \mathcal{G}_k = \left(\frac{2 G_c \ell_*^4}{D w_*^2}\right)^{1/2}, \quad \mathcal{G}_s = \frac{\sigma_0 \ell_*^4}{w_* D}. \tag{3.6a–c}$$

The scales ℓ_* and w_* are identified by imposing $\mathcal{G}_m = \mathcal{G}_s = 1$. This particular choice of scaling makes it possible to consider the limiting case $G_c = 0$. Hence,

$$\ell_* = \left(\frac{\mu' v D^2}{\sigma_0^3}\right)^{1/7}, \quad w_* = \left(\frac{\mu'^4 v^4 D}{\sigma_0^5}\right)^{1/7}, \tag{3.7a,b}$$

and the scale k_* for the curvature is therefore

$$k_* = \left(\frac{\mu'^2 v^2 \sigma_0}{D^3}\right)^{1/7}. \tag{3.8}$$

In addition, choosing

$$\alpha = 2 \tag{3.9}$$

guarantees that Ω remains bounded when $\gamma_f \to \infty$. Indeed, for this limit, the right-hand side of (3.2) vanishes (equivalent to an inviscid fluid), (3.3) effectively disappears as $\Lambda \to 0$, $\Omega(1) \to 0$ and importantly the curvature tends to a finite limit at $\xi = 1$.

Using the Euler–Bernoulli equation (2.1) and the continuity equation (2.11), the net pressure and flux scale according to

$$\Pi = \frac{\gamma_f^2 p}{p_*}, \quad \Psi = \frac{q}{\gamma_f^2 q_*}, \tag{3.10a,b}$$

with the scales p_* and q_* given by

$$p_* = \sigma_0, \quad q_* = \left(\frac{\mu'^4 v^{11} D}{\sigma_0^5}\right)^{1/7}. \tag{3.11a,b}$$

The above expressions for Π and Ψ guarantee that the scaled versions of (2.1) and (2.2) become

$$\frac{\mathrm{d}^4\Omega}{\mathrm{d}\xi^4} = \Pi, \quad \Psi = \Omega. \tag{3.12a,b}$$

https://doi.org/10.1017/jfm.2021.328 Published online by Cambridge University Press

Finally, the horizontal component H and the vertical component V of the force on the blade scale according to

$$\mathring{\mathcal{H}} = \frac{H}{H_*}, \quad \mathring{\mathcal{V}} = \frac{\gamma_f V}{V_*}, \tag{3.13a,b}$$

with the scales H_* and V_* given by

$$H_* = \left(\mu'^4 v^4 D \sigma_0^2\right)^{1/7}, \quad V_* = \left(\mu' v D^2 \sigma_0^4\right)^{1/7}. \tag{3.14a,b}$$

The scaling of the vertical force V is consistent with that of the net pressure, i.e. $V_* = \ell_* p_*$. It implies that for a long blister, the vertical force essentially equilibrates the pressure at the back end of the blister.

The remaining free number $\mathcal{G}_k$ in the original set (3.6*a–c*) can be interpreted as a dimensionless toughness; it is renamed as $\mathcal{K}$. For non-zero w_0, there is an additional number $\mathcal{W} = w_0/w_*$ controlling the back-end boundary layer. The front-end boundary layer only depends on $\mathcal{K}$, however, as the only information from the back end affecting its solution is the velocity v of the blade. In § 4.4, it is shown that the back-end boundary layer actually depends on a single number, a function of both $\mathcal{K}$ and $\mathcal{W}$. The explicit expressions of these two numbers in terms of the physical quantities defining the blister problem are given by

$$\mathcal{K} = \left(\frac{2^7 G_c^7}{D\sigma_0^2 \mu'^4 v^4}\right)^{1/14}, \quad \mathcal{W} = \left(\frac{w_0^7 \sigma_0^5}{\mu'^4 v^4 D}\right)^{1/7}. \tag{3.15a,b}$$

4. Long-blister limit

4.1. *Structure of solution*

As noted earlier, the dimensionless viscosity effectively vanishes in the interval $\xi \in [0, 1]$ and the lag Λ/γ_f tends to zero (noting that $\Lambda = O(1)$ or less, see following) for large γ_f. Viewed at length scale $\ell_f = \gamma_f \ell_*$, this solution is characterised by a uniform pressure $\mathring{\Pi}$. However, there exist two boundary layers, one at the advancing front and the other at the receding end of the blister, where viscous dissipation cannot be neglected, see figure 2. The solution in these (three) regions will be expressed as $\hat{\Omega}(\hat{\xi})$ for the front-end boundary layer, $\mathring{\Omega}(\xi)$ for the core region, and $\check{\Omega}(\check{\xi})$ for the back-end boundary layer. The boundary-layer solutions and the outer solution are matched with the curvature, which is equal to $\Upsilon(\mathcal{K})$ at both ends of the core region owing to the symmetric nature of the outer solution.

4.2. *Front-end boundary layer*

The boundary layer at the moving front is representative of the tip region of any propagating near-surface hydraulic fracture, provided that there is a separation of scales. The solution is expressed as $\hat{\Omega}(\hat{\xi})$, where

$$\hat{\xi} = (\ell - x)/\ell_*, \quad \hat{\Omega} = w/w_*, \tag{4.1a,b}$$

with the scales defined in (3.7*a,b*). The solution is characterised by a lag Λ, which, in the context of the moving blister, is equal to $\Lambda = (\ell - \ell_f)/\ell_*$. Its maximum value

https://doi.org/10.1017/jfm.2021.328 Published online by Cambridge University Press

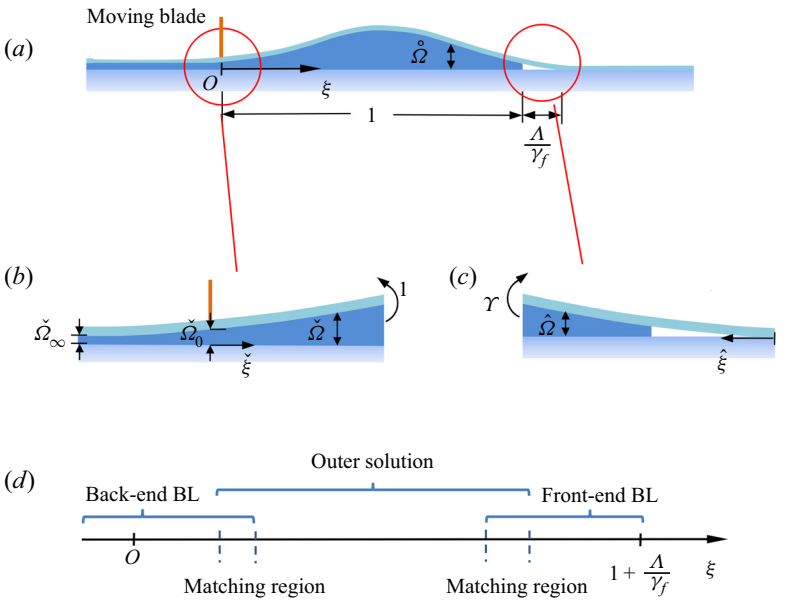

Figure 2. Structure of solution: (*a*) outer solution, (*b*) back-end boundary layer, (*c*) front-end boundary layer and (*d*) schematic of the regions of validity of the inner and outer solutions in the matching procedure.

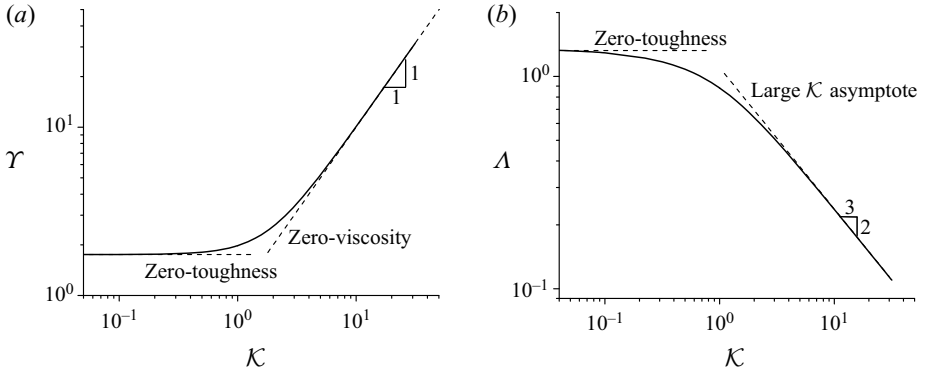

Figure 3. Front-end boundary layer: (*a*) far-field curvature Υ and (*b*) lag Λ; numerical solution (solid line) and asymptotic solution (dashed lines) (Wang & Detournay 2018).

$\Lambda_{max} = 1.325$ is reached in the limit $\mathcal{K} = 0$ (Wang & Detournay 2018). The far-field curvature $\Upsilon(\mathcal{K})$ is defined as

$$\Upsilon = \lim_{\hat{\xi}\to\infty} \hat{\Omega}'', \tag{4.2}$$

where the prime denotes differentiation with respect to the argument of the function. Plots of the functions $\Upsilon(\mathcal{K})$ and $\Lambda(\mathcal{K})$ are shown in figure 3. Since the curvature is matched between the outer solution and the front-end boundary layer, $\Upsilon(\mathcal{K})$ effectively represents the dimensionless toughness for the outer solution. This apparent toughness accounts not only for the energy expended in delamination at the front, but also for the resistance to propagation associated with the presence of a lag and for viscous dissipation in the tip region.

https://doi.org/10.1017/jfm.2021.328 Published online by Cambridge University Press

There are two limiting regimes of propagation (Ball & Neufeld 2018; Wang & Detournay 2018): a toughness-dominated regime ($\mathcal{K} \gtrsim 10$), and a viscosity-dominated regime ($\mathcal{K} \lesssim 0.1$). The asymptotic behaviours of $\Upsilon(\mathcal{K})$ for small and large $\mathcal{K}$ are given by

$$\Upsilon \simeq \mathcal{K}, \quad \mathcal{K} \gtrsim 10 \quad \text{and} \quad \Upsilon \simeq 1.769, \quad \mathcal{K} \lesssim 0.1 \tag{4.3a,b}$$

and in the range $0.1 < \mathcal{K} < 10$, $\Upsilon(\mathcal{K})$ is conveniently approximated as (Wang & Detournay 2018)

$$\Upsilon \simeq \sum_{i=0}^{4} a_i \mathcal{K}^i, \quad 0.1 < \mathcal{K} < 10, \tag{4.4}$$

where $a_0 = 1.70404$, $a_1 = 0.09348$, $a_2 = 0.21373$, $a_3 = -0.02278$ and $a_4 = 8.87789 \times 10^{-4}$.

4.3. *Outer solution*

The solution in the bulk of the blister, the outer solution, is denoted as $\mathring{\Omega}(\xi)$ and $\mathring{\Pi}$. These field variables are scaled similarly to $\Omega(\xi)$ and $\Pi(\xi)$. The outer solution is obtained by solving

$$\mathring{\Omega}'''' = \mathring{\Pi}, \quad \xi \in [0, 1], \tag{4.5}$$

with conditions

$$\mathring{\Omega} = \mathring{\Omega}' = 0, \quad \mathring{\Omega}'' = \Upsilon(\mathcal{K}), \quad \text{at } \xi = 1, \tag{4.6a,b}$$

$$\mathring{\Omega} = 0, \quad \mathring{\Omega}' = 0, \quad \text{at } \xi = 0. \tag{4.7a,b}$$

The solution is given by

$$\mathring{\Omega} = \frac{\mathring{\Pi}}{24}\xi^2(1-\xi)^2, \quad \mathring{\Pi} = 12\,\Upsilon(\mathcal{K}). \tag{4.8a,b}$$

The condition on the curvature at $\xi = 1$ is the matching condition between the outer solution and the front-end boundary layer. Because of the symmetry in $\mathring{\Omega}(\xi)$, the curvature at $\xi = 0$ is also equal to $\Upsilon(\mathcal{K})$. The curvature is further used to match the outer solution and the boundary-layer solution at the back end.

Although the curvature scale does not depend on γ_f, this dimensionless parameter enters the scales used to define ξ, $\mathring{\Omega}$ and $\mathring{\Pi}$. The blister thickness w and pressure p evolve therefore with time because γ_f decreases with t owing to the bleeding of the blister when $w_0 > 0$. However, the curvature at both ends of the blister is quasi-time-invariant as long as γ_f is large enough to guarantee that the front velocity $v' \simeq v$.

4.4. *Back-end boundary layer*

For the receding end of the blister, we introduce the fast variable $\check{\xi}$ and the associated blister thickness $\check{\Omega}(\check{\xi})$ and pressure $\check{\Pi}(\check{\xi})$

$$\check{\xi} = \Upsilon^3(\mathcal{K})\frac{x}{\ell_*}, \quad \check{\Omega} = \Upsilon^5(\mathcal{K})\frac{w}{w_*}, \quad \check{\Pi} = \Upsilon^{-7}(\mathcal{K})\frac{p}{p_*}. \tag{4.9a–c}$$

https://doi.org/10.1017/jfm.2021.328 Published online by Cambridge University Press

In this scaling, the horizontal force $\check{\mathcal{H}}$ and the vertical force $\check{\mathcal{V}}$ applied by the blade are naturally defined as

$$\check{\mathcal{H}} = \Upsilon^{-2}(\mathcal{K})\frac{H}{H_*}, \quad \check{\mathcal{V}} = \Upsilon^{-4}(\mathcal{K})\frac{V}{V_*}, \tag{4.10a,b}$$

so that $\check{\mathcal{H}} = -\check{\Omega}'(0)[\check{\Omega}'''(0)]$, $\check{\mathcal{V}} = -[\check{\Omega}'''(0)]$. The receding boundary layer and the outer solution are matched with the curvature, i.e.

$$\lim_{\xi\to 0} \mathring{\Omega}'' = \Upsilon(\mathcal{K}) \lim_{\check{\xi}\to\infty} \check{\Omega}'', \tag{4.11}$$

which implies that

$$\check{\Omega} = \tfrac{1}{2}\check{\xi}^2, \quad \check{\xi} \to \infty. \tag{4.12}$$

With the introduction of Υ in the definition of the boundary-layer variables, the system of equations governing $\check{\Omega}(\check{\xi})$ only depends on $\check{\Omega}_0$, the scaled gap at the blade

$$\check{\Omega}_0 = \mathcal{W}\Upsilon^5(\mathcal{K}). \tag{4.13}$$

The boundary layer consists of two parts: the back end of the blister corresponding to $\check{\xi} \in [0, \infty]$ and the tail behind the blade, $\check{\xi} \in [-\infty, 0]$. It can be deduced from (2.3) and (2.12) that the gap $\check{\Omega}(\check{\xi})$ in the boundary layer is governed by

$$\check{\Omega}^3\check{\Omega}'''' = -(\check{\Omega} - \check{\Omega}_\infty), \quad \check{\xi} \in [-\infty, \infty], \tag{4.14}$$

subject to the conditions

$$\check{\Omega} = \tfrac{1}{2}\check{\xi}^2 \quad \text{as } \check{\xi} \to \infty, \tag{4.15}$$

$$\check{\Omega} = \check{\Omega}_0 \quad \text{at } \check{\xi} = 0, \tag{4.16}$$

$$\check{\Omega} = \check{\Omega}_\infty \quad \text{as } \check{\xi} \to -\infty. \tag{4.17}$$

The system of (4.14)–(4.17) is closed as there are enough constraints to identify the five constants of integration for (4.14), the discontinuity of $\check{\Omega}'''(\check{\xi})$ at $\check{\xi} = 0$ and the residual gap $\check{\Omega}_\infty$. Indeed, (4.15) implies that $\check{\Omega}'' = 1$ and $\check{\Omega}''' = \check{\Omega}'''' = 0$ at $\check{\xi} = \infty$, while (4.17) entails the vanishing of the derivatives of $\check{\Omega}(\check{\xi})$ at $\check{\xi} = -\infty$.

Numerical solution of the system of (4.14)–(4.17) is facilitated by recognising that the governing equation (4.14) for the gap degenerates into a linear ODE at sufficiently large distance behind the blade

$$\check{\Omega}_\infty^3\check{\Omega}'''' = -(\check{\Omega} - \check{\Omega}_\infty), \quad -\check{\xi} \gg 1. \tag{4.18}$$

After dropping the terms that become unbounded as $\check{\xi} \to -\infty$, the asymptotic solution is thus given by

$$\check{\Omega} = \check{\Omega}_\infty + \left[\check{c}_1 \cos\left(\frac{\alpha\check{\xi}}{\check{\Omega}_\infty^{3/5}}\right) + \check{c}_2 \sin\left(\frac{\alpha\check{\xi}}{\check{\Omega}_\infty^{3/5}}\right)\right] \exp\left(\frac{\beta\check{\xi}}{\check{\Omega}_\infty^{3/5}}\right), \quad -\check{\xi} \gg 1, \tag{4.19}$$

where

$$\alpha = \sqrt{\frac{5}{8} - \frac{\sqrt{5}}{8}}, \quad \beta = \left(\frac{1}{4} + \frac{\sqrt{5}}{4}\right). \tag{4.20a,b}$$

The above asymptotic solution replaces the boundary condition (4.17) at $\check{\xi} = -\infty$. Now nine conditions are needed to obtain a solution: five to integrate the ODE, one to determine

https://doi.org/10.1017/jfm.2021.328 Published online by Cambridge University Press

$[\check{\Omega}'''(0)]$ and three to identify the unknowns $\check{\Omega}_\infty$, $\check{c}_1$, and $\check{c}_2$ of the asymptotic solution. These requirements are fulfilled by the three conditions equivalent to (4.15) as $\check{\xi} \to \infty$, one constraint at $\check{\xi} = 0$ and five continuity conditions with the asymptotic solution (4.19), namely the function $\check{\Omega}(\check{\xi})$ and its first four derivatives at the truncated boundary.

The solution in the back-end boundary layer is obtained numerically by combining a finite-element discretisation of the beam equation and a finite-volume discretisation of the lubrication equation. The general algorithm is the same as the one used to solve the front-end boundary layer, see Wang & Detournay (2018) for details. The infinite fluid-filled channel is truncated to the interval $\check{\xi} \in [\check{\xi}_{-\infty}, \check{\xi}_\infty]$, where $\check{\xi}_{-\infty}$ and $\check{\xi}_\infty$ are chosen, through a trial-and-error procedure, to be large enough to ensure convergence of the solution. The finite region is divided into n elements that are delimited by $n+1$ nodes with coordinate $\check{\xi}_i$, $i = 1, \ldots, n+1$. One node is located at $\check{\xi} = 0$ enabling us to impose the constraint $\check{\Omega}(0) = \check{\Omega}_0$. Net pressure $\check{\Pi}_i$, aperture $\check{\Omega}_i$ and aperture gradient $\check{\Omega}'_i$ are the primarily variables defined at each node $i = 1, \ldots, n+1$, while flux $\check{\Psi}_{i+1/2}$ is evaluated at the midpoint of element i. The discretised fluid–beam equations and the boundary conditions constitute a system of $2n+2$ nonlinear algebraic equations in terms of $2n+2$ unknowns $\check{\Omega}_\infty, \check{c}_1, \check{c}_2, \check{\Omega}_i, \check{\Omega}'_i$, $i = 2, \ldots, n+1$ (except for the opening at $\check{\xi} = 0$), noting that $\check{\Omega}_1, \check{\Omega}'_1$ are determined by the constants $\check{\Omega}_\infty$, $\check{c}_1$ and $\check{c}_2$. These nonlinear systems of equations are solved using Newton's iteration procedure built in the Mathematica software.

5. Small-, intermediate- and large-$\check{\Omega}_0$ regimes

Motivated by the determination of the force on the blade, we focus our attention to the structure of the solution near the origin. As evident from the system of (4.14)–(4.17), the scaled solution in the back-end boundary layer depends on only one number, the prescribed gap $\check{\Omega}_0 = \mathcal{W}\Upsilon^5(\mathcal{K})$ at the blade edge. In principle, we can identify three regimes: (i) a small-$\check{\Omega}_0$ asymptote, which only depends on the viscous dissipation in the receding boundary layer; (ii) an intermediate-$\check{\Omega}_0$ regime; (iii) a large-$\check{\Omega}_0$ asymptote for which the curvature in front of the blade is equal to the matched curvature between the front-end boundary layer and the bulk solution.

5.1. *Small-$\check{\Omega}_0$ regime*

If $\check{\Omega}_0 = 0$, the blister thickness $\check{\Omega}(\check{\xi})$ near $\check{\xi} = 0$ is given by (Tayler & King 1987)

$$\check{\Omega} \overset{\check{\xi}\to 0}{\sim} A\check{\xi}^{5/3}, \tag{5.1}$$

with

$$A = \frac{1}{2}\left(\frac{3^5}{5\times 7}\right)^{1/3} \simeq 0.9539 \tag{5.2}$$

as it can be confirmed by substituting this power-law solution into (4.14).

When $\check{\Omega}_0 \ll 1$, $\check{\Omega} = A\check{\xi}^{5/3}$ becomes an intermediate asymptotic. To determine the solution near the origin, the problem can be rescaled so that this asymptote applies to

https://doi.org/10.1017/jfm.2021.328 Published online by Cambridge University Press

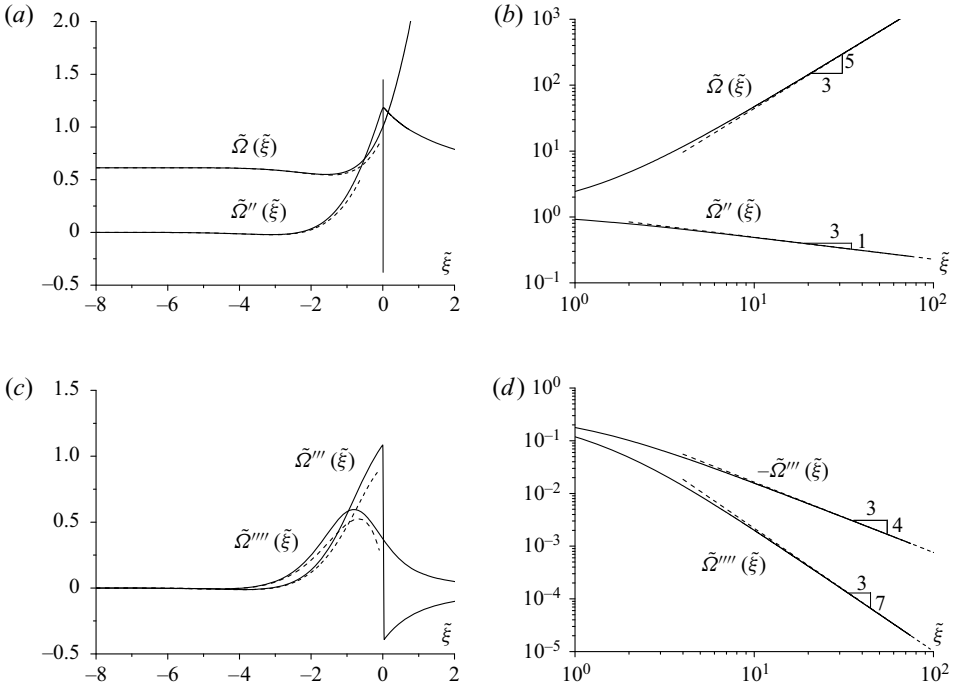

Figure 4. Numerical (solid line) and asymptotic (dashed line) small-$\check{\Omega}_0$ solutions near the back end: (*a*,*b*) gap $\tilde{\Omega}(\tilde{\xi})$ and curvature $\tilde{\Omega}''(\tilde{\xi})$; (*c*,*d*) shear force $\tilde{\Omega}'''(\tilde{\xi})$ and net fluid pressure $\tilde{\Omega}''''(\tilde{\xi})$.

the far field in the rescaled variable. This is done by introducing the new scaling

$$\tilde{\xi} = \check{\Omega}_0^{-3/5}\check{\xi}, \quad \tilde{\Omega} = \check{\Omega}_0^{-1}\check{\Omega}, \quad \tilde{\Pi} = \check{\Omega}_0^{7/5}\check{\Pi}. \tag{5.3a–c}$$

The gap aperture $\tilde{\Omega}(\tilde{\xi})$ is then governed by

$$\tilde{\Omega}^3\tilde{\Omega}'''' = -(\tilde{\Omega} - \tilde{\Omega}_\infty), \quad \tilde{\xi} \in [-\infty, \infty], \tag{5.4}$$

with conditions

$$\tilde{\Omega} \overset{\tilde{\xi}\to\infty}{\sim} A\tilde{\xi}^{5/3}, \tag{5.5}$$

$$\tilde{\Omega} = 1 \quad \text{at } \tilde{\xi} = 0, \tag{5.6}$$

$$\tilde{\Omega} = \tilde{\Omega}_\infty + \left[\tilde{c}_1 \cos\left(\frac{\alpha\tilde{\xi}}{\tilde{\Omega}_\infty^{3/5}}\right) + \tilde{c}_2 \sin\left(\frac{\alpha\tilde{\xi}}{\tilde{\Omega}_\infty^{3/5}}\right)\right] \exp\left(\frac{\beta\tilde{\xi}}{\tilde{\Omega}_\infty^{3/5}}\right), \qquad -\tilde{\xi} \gg 1, \tag{5.7}$$

where $\tilde{\Omega}_\infty = \check{\Omega}_\infty/\check{\Omega}_0$ is an *a priori* unknown number (smaller than 1). In other words, $\check{\Omega}_\infty$ is simply proportional to $\check{\Omega}_0$ in the asymptotic small-$\check{\Omega}_0$ regime.

The system of (5.4)–(5.7) is solved numerically using an approach similar to that described in § 4.4. The asymptotic solution (5.5) is replaced by imposing the second, third and fourth derivative of (5.5) at a point $\tilde{\xi}_\infty \gg 1$. Point $\tilde{\xi}_\infty$ must be chosen in such a way that the computed $\tilde{\Omega}$ matches (5.5) in the neighbourhood of $\tilde{\xi}_\infty$. A similar approach is used for the continuity conditions between the computed $\tilde{\Omega}$ and (5.7), which is enforced at a

https://doi.org/10.1017/jfm.2021.328 Published online by Cambridge University Press

point $-\tilde{\xi}_\infty \gg 1$. Numerical solution of (5.4)–(5.7) yields $\tilde{\Omega}_\infty = 0.6125$, $\tilde{\Omega}'(0) = 0.8558$, $\tilde{\Omega}''(0) = 1.195$, $[\tilde{\Omega}'''(0)] = -1.430$ and $\tilde{\Omega}''''(0) = 0.3732$.

The small-$\check{\Omega}_0$ asymptotic solution is illustrated in figure 4 ($\tilde{\Omega}(\tilde{\xi})$, $\tilde{\Omega}''(\tilde{\xi})$, $\tilde{\Omega}'''(\tilde{\xi})$ and $\tilde{\Omega}''''(\tilde{\xi})$) in a linear scale near the origin to capture the solution behind the blade and in double logarithmic scale to illustrate convergence of the solution to the intermediate asymptote (5.5) in the back end of the blister. These figures indicate that the asymptotic solution (5.7) is effectively reached at $\tilde{\xi} \simeq -4$, and that the numerical solution matches the intermediate asymptote (5.5) at approximately $\tilde{\xi} \simeq 10$. In particular, note that the minimum gap $\tilde{\Omega}_{min} = 0.5495$ is located at $\tilde{\xi}_{min} = -1.566$. The peak pressure occurs at $\tilde{\xi} = -0.8052$, which marks the transition between forward and backward average flow.

There is another solution operating on the scale of the variable $\check{\xi}$ that connects the (intermediate) asymptote (5.1) to the far-field quadratic condition (4.12). This solution would need to be computed numerically. However, the intermediate asymptote (5.1) effectively shields the solution $\tilde{\Omega}(\tilde{\xi})$ from (4.12), and thus from the processes at the front of the blister. In other words, the reaction force on the blade only depends on the viscous dissipation at the back end of the blister in the small-$\check{\Omega}_0$ regime.

5.2. *Large-$\check{\Omega}_0$ regime*

In the large-$\check{\Omega}_0$ regime, viscous dissipation is expected to be negligible in the neighbourhood of the blade. Completely ignoring viscous effects, which implies a zero net pressure, would cause, however, the elastic sheet to contact the rigid substrate at some distance behind the blade (see the outer solution illustrated in the inset of figure 5*a*). However, as indicated earlier, the viscous dissipation associated with the narrowing of the gap leads to an increase of the fluid pressure. Complete closure of the gap is actually prevented, as it would entail a strong pressure singularity according to (5.1). This contradiction suggests the existence of an asymptotic viscous layer inside the back-end boundary layer, with the zero-viscosity solution acting as an outer solution.

5.2.1. *Outer solution*

A rescaling of the boundary-layer variables is required to derive the zero-viscosity solution. After defining the new variables as

$$\bar{\xi} = \check{\Omega}_0^{-1/2}\check{\xi}, \quad \bar{\Omega} = \check{\Omega}_0^{-1}\check{\Omega}, \tag{5.8a,b}$$

so as to preserve the independence upon $\check{\Omega}_0$ of the constant curvature at infinity, the governing equation becomes

$$\bar{\Omega}^3\bar{\Omega}'''' = -\check{\Omega}_0^{-1/2}\left(\bar{\Omega} - \bar{\Omega}_\infty\right), \quad \bar{\xi} \in [-\infty, \infty], \tag{5.9}$$

with $\bar{\Omega}_\infty = \check{\Omega}_\infty/\check{\Omega}_0$. This equation indicates that the right-hand side is negligibly small and can thus be ignored provided that $\check{\Omega}_0 \gg 1$ and $\bar{\Omega}$ is of order $O(1)$ or more. Noting the condition at infinity, the zero-order solution $\bar{\Omega}_{(0)}(\bar{\xi})$ is obtained by solving

$$\bar{\Omega}_{(0)}'''' = 0, \quad \bar{\xi} \in \left[\bar{\xi}_c, \infty\right], \tag{5.10}$$

subjected to

$$\bar{\Omega}_{(0)}'' = 1,\ \bar{\Omega}_{(0)}''' = 0 \quad \text{at } \bar{\xi} = \infty; \quad \bar{\Omega}_{(0)}(0) = 1; \quad \bar{\Omega}_{(0)} = \bar{\Omega}_{(0)}' = \bar{\Omega}_{(0)}'' = 0 \quad \text{at } \bar{\xi} = \bar{\xi}_c. \tag{5.11a–d}$$

https://doi.org/10.1017/jfm.2021.328 Published online by Cambridge University Press

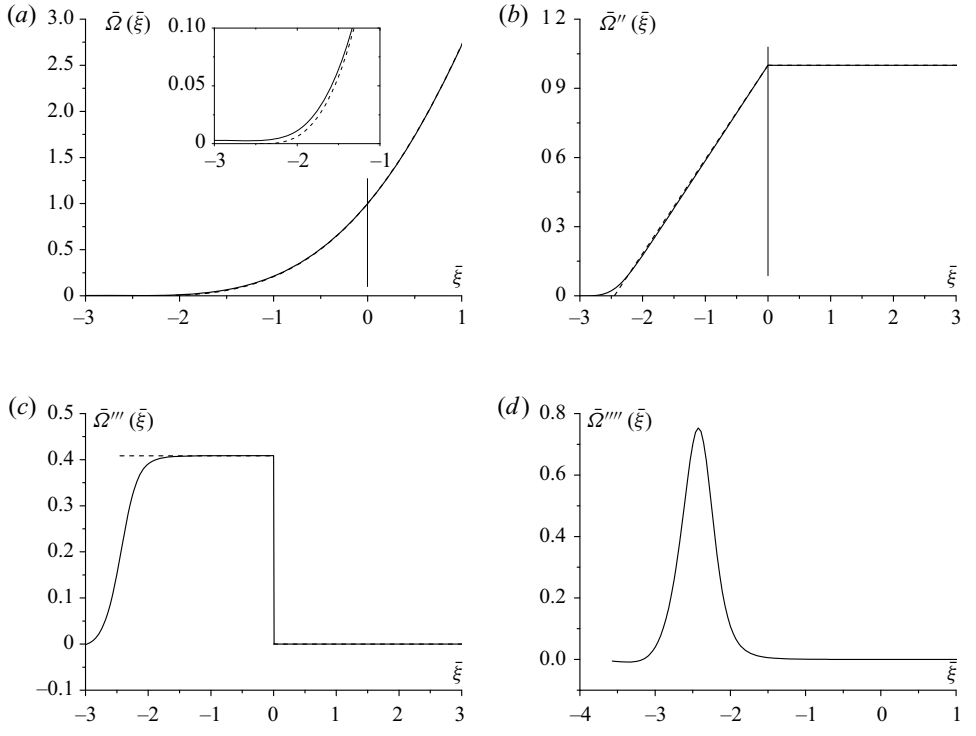

Figure 5. Numerical (solid line) and zero-order (dashed line) outer solution near the back end for large $\check{\Omega}_0$: (*a*) $\bar{\Omega}(\bar{\xi})$, (*b*) $\bar{\Omega}''(\bar{\xi})$, (*c*) $\bar{\Omega}'''(\bar{\xi})$ and (*d*) $\bar{\Omega}''''(\bar{\xi})$. Results calculated for $\check{\Omega}_0 = 6.4 \times 10^7$.

In the above, $\bar{\xi}_c < 0$ is the *a priori* unknown position of the contact line where the elastic sheet would touch the substrate if the fluid were inviscid. This set of equations is closed since the six conditions (5.11*a–c*) provide the necessary information to determine the four constants of integration, $[\bar{\Omega}'''_{(0)}(0)]$, and $\bar{\xi}_c$.

The zero-order solution $\bar{\Omega}_{(0)}(\bar{\xi})$ is readily obtained as

$$\bar{\Omega}_{(0)}(\bar{\xi}) = \begin{cases} 0, & \bar{\xi} \le -\bar{\xi}_c, \\ \left(\dfrac{\bar{\xi}_c - \bar{\xi}}{\bar{\xi}_c}\right)^3, & \bar{\xi}_c \le \bar{\xi} \le 0, \\ 1 + \dfrac{\bar{\xi}}{2}\left(\bar{\xi} - \bar{\xi}_c\right), & \bar{\xi} \ge 0, \end{cases} \tag{5.12}$$

with

$$\bar{\xi}_c = -\sqrt{6}. \tag{5.13}$$

The numerical solution of $\bar{\Omega}(\bar{\xi})$ in the large-$\check{\Omega}_0$ regime, which is governed by equations similar to the system (5.4)–(5.7) except for the condition as $\bar{\xi} \to \infty$, is illustrated in figure 5(*a*), together with the zero-order solution (5.12). Comparison between the numerical and the zero-order solution for $\bar{\Omega}''(\bar{\xi})$, $\bar{\Omega}'''(\bar{\xi})$ and $\bar{\Omega}''''(\bar{\xi})$ can be found in figure 5(*c*,*d*), noting that $\bar{\Omega}''''_{(0)}(\bar{\xi}) = 0$. Figure 5 reveals the existence of a nested boundary layer near $\bar{\xi} = \bar{\xi}_c$.

https://doi.org/10.1017/jfm.2021.328 Published online by Cambridge University Press

5.2.2. *Inner solution*

Yet another scaling is required to determine the solution in the inner viscous layer at the back end for the large-$\breve{\Omega}_0$ regime, in particular the relationship between $\breve{\Omega}_\infty$ and $\breve{\Omega}_0$. Thus, let

$$\breve{\xi} = (\bar{\xi} - \bar{\xi}_c)\breve{\Omega}_0^{\lambda}, \quad \breve{\Omega} = \bar{\Omega}\breve{\Omega}_0^{\nu}, \tag{5.14}$$

where the exponents λ and ν (expected to be positive) are to be specified by requiring that the equations governing $\breve{\Omega}(\breve{\xi})$ do not contain $\breve{\Omega}_0$. The information needed to determine these two power-law indices can be deduced from the rescaled governing equation

$$\breve{\Omega}_0^{5\lambda-3\nu+1/2}\breve{\Omega}^3\breve{\Omega}'''' = -\left(\breve{\Omega} - \breve{\Omega}_\infty\right) \tag{5.15}$$

and the condition

$$\breve{\Omega}_0^{3\lambda-\nu}\breve{\Omega}''' = -\bar{\xi}_c^{-1} \quad \text{as } \breve{\xi} \to \infty, \tag{5.16}$$

deduced by matching $\bar{\Omega}'''_{(0)}(0^-) = -\bar{\xi}_c^{-1}$ as $\breve{\xi} \to \infty$. Except for the finite (unknown) condition

$$\breve{\Omega} = \breve{\Omega}_\infty \equiv \frac{\breve{\Omega}_\infty}{\breve{\Omega}_0}\breve{\Omega}_0^{\nu} \quad \text{as } \breve{\xi} \to -\infty, \tag{5.17}$$

all the other conditions on $\breve{\Omega}(\breve{\xi})$ or its derivatives are either zero or infinite. Elimination of the exponents of $\breve{\Omega}_0$ in (5.15) and (5.16) requires $\lambda = 1/8$ and $\nu = 3/8$. These results further imply that

$$\breve{\Omega}_\infty = \breve{\Omega}_\infty\breve{\Omega}_0^{5/8}. \tag{5.18}$$

If the asymptotic solution (4.19), properly rescaled for $\breve{\Omega}(\breve{\xi})$, is used, there are eight unknowns: $\breve{\Omega}_\infty$, the two constants of the asymptotic solution (4.19) and five constants of integration. The problem is closed by the five continuity conditions between the asymptotic solution (4.19) and $\breve{\Omega}(\breve{\xi})$ and the asymptotic condition (5.16) as $\breve{\xi} \to \infty$. (The asymptotic condition can be construed as being equivalent to the three conditions $\breve{\Omega}''(\breve{\xi}_\infty) = -\bar{\xi}_c^{-1}\breve{\xi}_\infty$, $\breve{\Omega}'''(\breve{\xi}_\infty) = -\bar{\xi}_c^{-1}$ and $\breve{\Omega}''''(\breve{\xi}_\infty) = 0$, with $\breve{\xi}_\infty$ denoting the truncated boundary, when constructing the solution numerically.) The numerical solution in this viscous boundary layer can be found in figure 6, together with the asymptotic solution. Numerical results show that $\breve{\Omega}_\infty = 2.431$.

5.3. *Intermediate-$\breve{\Omega}_0$ regime*

The system of (4.14)–(4.15) can be solved numerically to construct the solution for intermediate values of $\breve{\Omega}_0$, which can then be connected to the small- and large-$\breve{\Omega}_0$ asymptotic solutions, recast in the original back-end boundary-layer scaling (4.9*a–c*).

Some of numerical results obtained by varying $\breve{\Omega}_0$ over the range $[10^{-2}$–$10^{8}]$ are compiled in figure 7. This figure illustrates the variation of $\breve{\Omega}'(0)$, $\breve{\Omega}_\infty$, $\breve{\mathcal{V}}$ and $\breve{\mathcal{H}}$ with $\breve{\Omega}_0$ together the asymptotic solutions, which are summarised in table 1. These results indicate that the large-$\breve{\Omega}_0$ asymptotic solution applies for $\breve{\Omega}_0 \gtrsim 10^5$ and the small-$\breve{\Omega}_0$ asymptotic solution for $\breve{\Omega}_0 \lesssim 10^{-1}$.

https://doi.org/10.1017/jfm.2021.328 Published online by Cambridge University Press

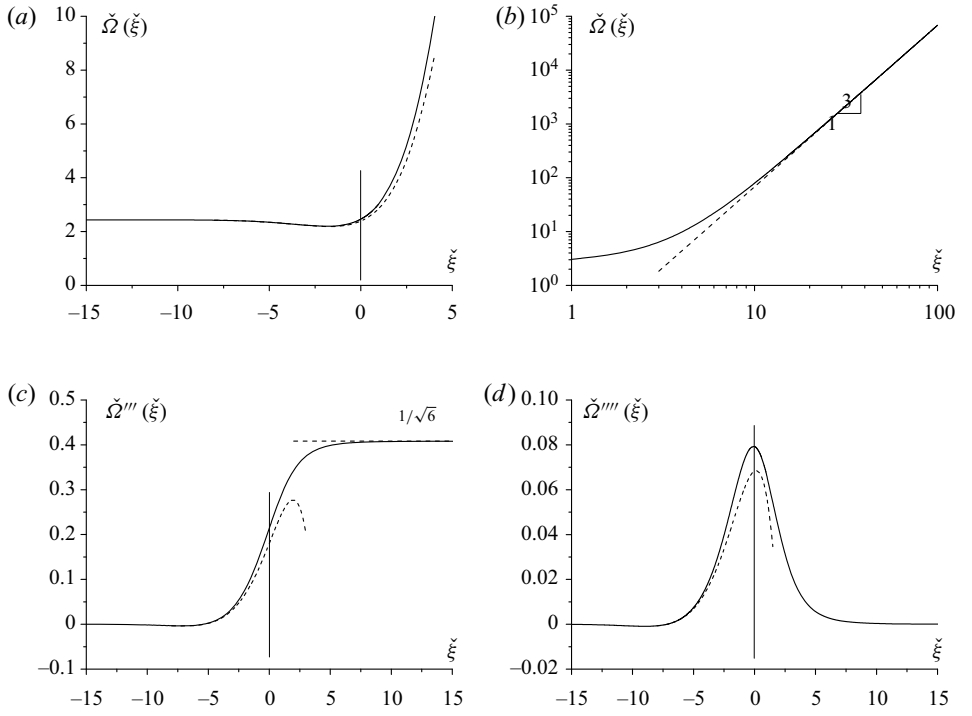

Figure 6. Numerical (solid line) and asymptotic (dashed line) solution in the viscous boundary layer in the neighbourhood of the blade for the large-$\check{\Omega}_0$ regime: (*a*,*b*) gap $\check{\Omega}(\check{\xi})$, (*c*) shear force $\check{\Omega}'''(\check{\xi})$ and (*d*) net pressure $\check{\Omega}''''(\check{\xi})$. Results calculated for $\check{\Omega}_0 = 6.4 \times 10^7$.

6. Force on the moving blade

While the relationships $\check{\mathcal{H}}(\check{\Omega}_0)$ and $\check{\mathcal{V}}(\check{\Omega}_0)$ illustrated in figure 7(*b*,*d*) in combination with the scales contain all the information needed to determine the magnitude of the horizontal force and the vertical force applied on the moving blade, it is useful to recast these results in terms of the scaled forces $\mathcal{H}(\mathcal{W}, \mathcal{K}) = H/H_*$ and $\mathcal{V}(\mathcal{W}, \mathcal{K}) = V/V_*$, noting that $\mathcal{H} = \Upsilon^2(\mathcal{K})\check{\mathcal{H}}$ and $\mathcal{V} = \Upsilon^4(\mathcal{K})\check{\mathcal{V}}$. The dependence of $\mathcal{H}$ and $\mathcal{V}$ on toughness $\mathcal{K}$ and gap $\mathcal{W}$ are illustrated in figure 8.

The horizontal force $\mathcal{H}$ can also be related to the dissipation in the fluid and at the separation front. The viscous dissipation in the back-end boundary layer is given by

$$\check{G}_f = -\int_{-\infty}^{\infty} \check{\Pi}'\check{\Psi}\,\mathrm{d}\check{\xi}. \tag{6.1}$$

Expressing the pressure $\check{\Pi}$ and the flux $\check{\Psi}$ in the previous equation in terms of $\check{\Omega}$ using the Euler–Bernoulli equation and the continuity equation yields

$$\check{G}_f = -\int_{-\infty}^{\infty} \check{\Omega}''''' \left(\check{\Omega} - \check{\Omega}_\infty\right) \mathrm{d}\check{\xi}. \tag{6.2}$$

Noting the conditions (4.15)–(4.17) and integrating by parts three times leads to

$$\check{G}_f = -\tfrac{1}{2} - \check{\Omega}'(0)\left[\check{\Omega}'''(0)\right], \tag{6.3}$$

https://doi.org/10.1017/jfm.2021.328 Published online by Cambridge University Press

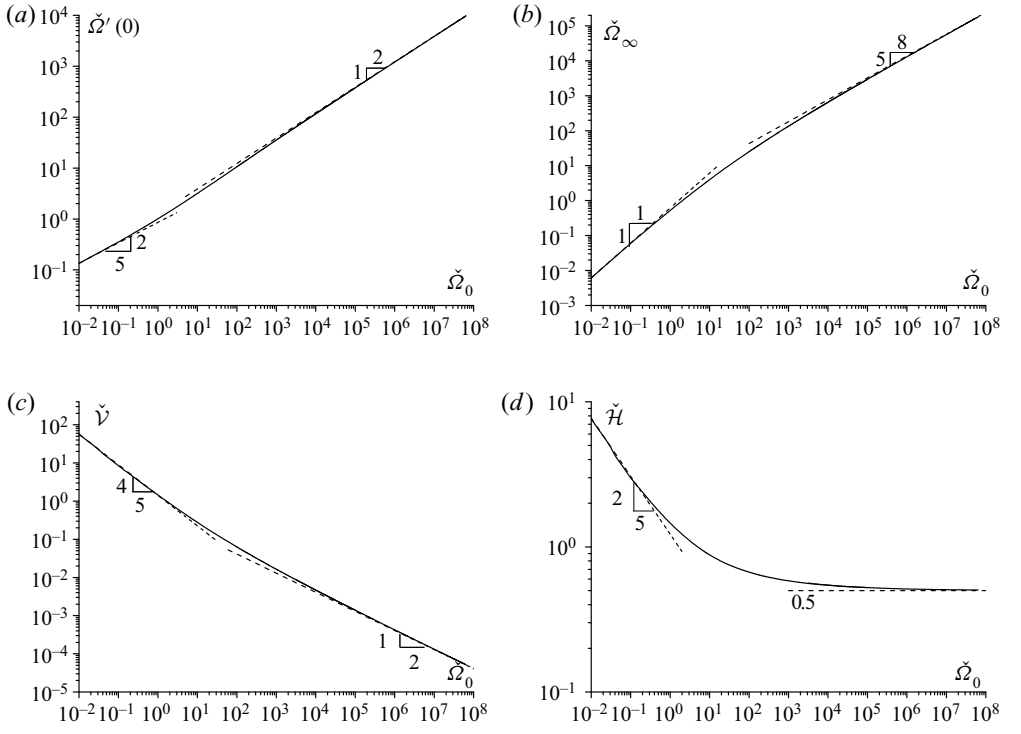

Figure 7. Variation of (*a*) slope $\check{\Omega}'(0)$, (*b*) residual gap $\check{\Omega}_\infty$, (*c*) force component $\check{\mathcal{V}}$ and (*d*) force component $\check{\mathcal{H}}$ with $\check{\Omega}_0$. Numerical (solid line) and asymptotic (dashed line) solutions.

	Small-$\check{\Omega}_0$	Large-$\check{\Omega}_0$
$\check{\Omega}_\infty$	$0.6125\check{\Omega}_0$	$2.431\check{\Omega}_0^{5/8}$
$\check{\Omega}'(0)$	$0.8558\check{\Omega}_0^{2/5}$	$\frac{3}{\sqrt{6}}\check{\Omega}_0^{1/2}$
$\check{\mathcal{V}}$	$1.430\check{\Omega}_0^{-4/5}$	$\frac{1}{\sqrt{6}}\check{\Omega}_0^{-1/2}$
$\check{\mathcal{H}}$	$1.224\check{\Omega}_0^{-2/5}$	$\frac{1}{2}$

Table 1. Summary of asymptotes.

which can be rewritten as

$$\mathcal{H} = \mathcal{D}_c + \mathcal{D}_f, \tag{6.4}$$

where $\mathcal{D}_c = \Upsilon^2/2$, $\mathcal{D}_f = \Upsilon^2\check{G}_f$. This equation is an expression of the energy balance: the external power $v\mathcal{H}$ is balanced by dissipation $v\mathcal{D}_c$ at the front end of the blister (a combination of dissipation in the fluid and at the separation front) and by viscous dissipation $v\mathcal{D}_f$ at the back end.

In the small-$\check{\Omega}_0$ regime, the horizontal force $\mathcal{H}$ simplifies to

$$\mathcal{H} = 1.224\mathcal{W}^{-2/5}, \quad \check{\Omega}_0 \lesssim 10^{-1}, \tag{6.5}$$

https://doi.org/10.1017/jfm.2021.328 Published online by Cambridge University Press

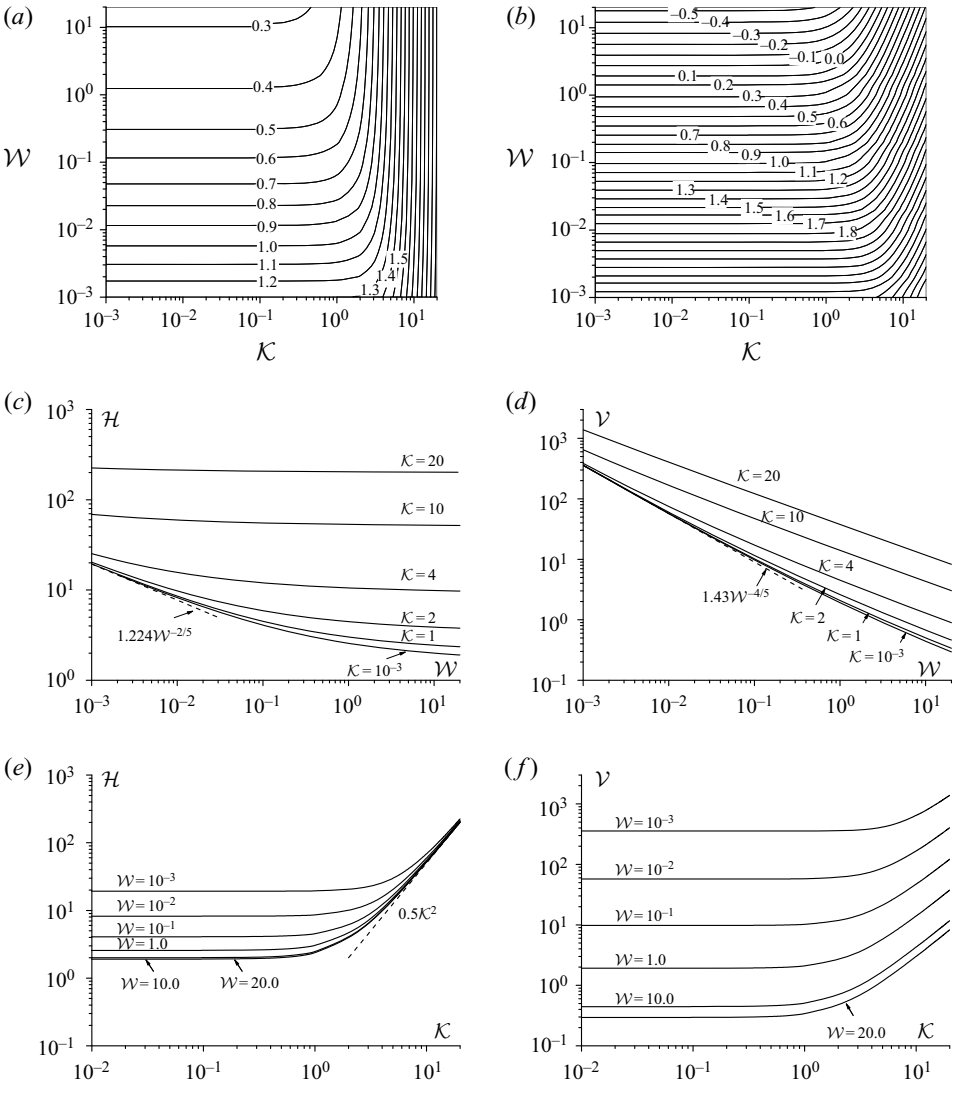

Figure 8. Force at the blister back end: (*a*) $\log_{10}(\mathcal{H})$ as a function of $\mathcal{K}$ and $\mathcal{W}$; (*b*) $\log_{10}(\mathcal{V})$ as a function of $\mathcal{K}$ and $\mathcal{W}$; (*c*) $\mathcal{H}$ as a function of $\mathcal{W}$; (*d*) $\mathcal{V}$ as a function of $\mathcal{W}$; (*e*) $\mathcal{H}$ as a function of $\mathcal{K}$; (*e*) $\mathcal{V}$ as a function of $\mathcal{K}$. Numerical solution (solid line) and asymptotic solution (dashed line).

and the vertical force $\mathcal{V}$ to

$$\mathcal{V} = 1.43\mathcal{W}^{-4/5}, \quad \check{\Omega}_0 \lesssim 10^{-1}. \tag{6.6}$$

In the large-$\check{\Omega}_0$ regime

$$\mathcal{H} = \tfrac{1}{2}\Upsilon^2(\mathcal{K}), \quad \check{\Omega}_0 \gtrsim 10^6, \tag{6.7}$$

and

$$\mathcal{V} = \tfrac{1}{\sqrt{6}}\Upsilon^{3/2}\mathcal{W}^{-1/2}, \quad \check{\Omega}_0 \gtrsim 10^6. \tag{6.8}$$

https://doi.org/10.1017/jfm.2021.328 Published online by Cambridge University Press

As a result, the relationship between H, V and the blade velocity v depends on the regime.

(i) Small-$\breve{\Omega}_0$ asymptotics. The horizontal force is given by

$$H = 1.224\left(\frac{D\mu'^4 v^4}{w_0^2}\right)^{1/5}, \quad \breve{\Omega}_0 \lesssim 10^{-1}, \tag{6.9}$$

and the vertical force by

$$V = 1.43\left(\frac{D^2\mu'^3 v^3}{w_0^4}\right)^{1/5}, \quad \breve{\Omega}_0 \lesssim 10^{-1}. \tag{6.10}$$

These expressions indicate that $H \sim v^{4/5}$ and $V \sim v^{3/5}$. The magnitude of the applied force is only related to the viscous dissipation near the receding end.

(ii) Large-$\breve{\Omega}_0$ asymptotics: $\mathcal{W}\Upsilon^5(\mathcal{K}) \gtrsim 10^6$. The force is controlled by processes at the leading edge of the blister. In the toughness-dominated regime at the propagating front, the applied forces are independent of the velocity v

$$H = G_c, \quad \text{if } \mathcal{K} \gtrsim 10 \text{ and } \mathcal{W} \gtrsim 10^6\mathcal{K}^{-5}, \tag{6.11}$$

$$V = \frac{1}{\sqrt{3}}\left(\frac{2G_c^3 D}{w_0^2}\right)^{1/4}, \quad \text{if } \mathcal{K} \gtrsim 10 \text{ and } \mathcal{W} \gtrsim 10^6\mathcal{K}^{-5}. \tag{6.12}$$

On the other hand, if the regime of propagation is viscosity dominated at the front, then

$$H = 1.565\left(D\mu'^4 v^4 \sigma_0^2\right)^{1/7}, \quad \text{if } \mathcal{K} \lesssim 0.1 \text{ and } \mathcal{W} \gtrsim 5.77 \times 10^4, \tag{6.13}$$

and

$$V = 0.961\left(\frac{D^5\mu'^6 v^6 \sigma_0^3}{w_0^7}\right)^{1/14}, \quad \text{if } \mathcal{K} \lesssim 0.1 \text{ and } \mathcal{W} \gtrsim 5.77 \times 10^4. \tag{6.14}$$

Thus, $H \sim v^{4/7}$ and $V \sim v^{3/7}$ are independent of the adhesion energy G_c.

7. Conclusions

In this paper we have analysed the motion of a two-dimensional blister trapped between a rigid substrate and an adhering elastic sheet. In contrast to most problems involving the hydraulically forced peeling of an elastic sheet from its substrate, the fluid is driven here by a moving blade rather than by injection of fluid. The peculiarity of this problem lies further in regularisations of the solution at both ends of the blister, an advancing fluid front that lags behind the separation front and a residual fluid film behind the receding end of the blister. The main objective of the study was to determine, for a long blister, the dependence of the reaction force on the blade upon the problem parameters.

Through scaling, it was shown that the asymptotic solution depends on two dimensionless groups $\mathcal{K}$ and $\mathcal{W}$ that can be interpreted, respectively, as a toughness and as an imposed gap at the back end. This asymptotic solution reflects the existence of a quasi-uniform pressure region in the bulk of the blister. This central region is sandwiched

https://doi.org/10.1017/jfm.2021.328 Published online by Cambridge University Press

between two boundary layers, which can be approximated as travelling waves in the long blister limit. Furthermore, the solution in the front-end boundary layer, including the lag between the separation and the fluid fronts, only depends on $\mathcal{K}$ and thus is insensitive to the conditions at the receding back end of the blister, except for the blade velocity.

When matching asymptotes at the back end, information from the front-end boundary layer namely the matching curvature of the elastic sheet is transferred to the back end through the uniform pressure central region. This matched curvature is independent of the blister length. It is found that only one number $\check{\Omega}_0$, a rescaled residual aperture, controls the solution in the back-end boundary layer and thus the force on the blade. In the small-$\check{\Omega}_0$ regime, the back-end solution is characterised by the existence of an intermediate viscosity asymptote, which effectively shields the receding contact line from toughness $\mathcal{K}$. In this regime, the scaled force on the blade is dominated by viscous dissipation at the back end and is solely a function of the residual aperture $\mathcal{W}$. For the large-$\check{\Omega}_0$ asymptote, the curvature at the receding end is equal to the matched curvature between the advancing boundary layer and the bulk solution. In this regime, $\mathcal{H}$ only depends on toughness $\mathcal{K}$, whereas the vertical force $\mathcal{V}$ depends on both $\mathcal{K}$ and $\mathcal{W}$.

Relaxing the assumption of a long blister introduces a time dependency to the problem. As a result, the velocity of the separation front and of the fluid front become time dependent and are no longer the same as the blade velocity. Moreover, the front end is now coupled to the whole solution, including the back end with a feedback from the residual film thickness. These considerations should be accounted for in further investigations, including the membrane effect in the elastic sheet and the viscous shear stresses that have been ignored in this study.

Acknowledgements. Z.W. would like to acknowledge support from the China Scholarship Council and also from the MTS visiting Professorship in Geomechanics, which enabled the current research to be completed during visits to the University of Minnesota. Partial support of E.D. was provided by the T.W. Bennett Chair in Mining Engineering and Rock Mechanics. The authors are grateful for the critical comments and insight provided by three anonymous reviewers. They are particularly indebted to one reviewer who identified a conceptual mistake in the original manuscript, thus saving them from future embarrassment.

Declaration of interests. The authors report no conflict of interest.

Author ORCIDs.
Emmanuel Detournay https://orcid.org/0000-0003-3698-7575.

Appendix A. Estimation of the front velocity

In this appendix, the front velocity is estimated for a long blister that is bleeding fluid at its back end. The outer solution for a long blister is characterised by a uniform pressure $p(t)$. Further imposing $w = w' = 0$ at $x = 0$ and $x = \ell(t)$ leads to the following expression for the gap $w(x, t)$

$$w = \frac{p}{24D} x^2 (\ell(t) - x)^2, \tag{A1}$$

from which we deduce the beam curvature at $x = \ell(t)$

$$w''\big|_{x=\ell(t)} = \frac{p\ell^2(t)}{12D}. \tag{A2}$$

On the other hand, matching the outer curvature at $x = \ell(t)$ to the far-field curvature of the front-region boundary layer yields

$$w''\big|_{x=\ell(t)} = k_* \Upsilon(\mathcal{K}). \tag{A3}$$

https://doi.org/10.1017/jfm.2021.328 Published online by Cambridge University Press

The pressure $p(t)$ is then deduced by comparing (A2) and (A3)

$$p(t) = \frac{12D}{\ell^2(t)} k_* \Upsilon(\mathcal{K}). \tag{A4}$$

Neglecting the crack volume in the lag region, the fluid volume A_f trapped in the blister is given by

$$A_f = \int_0^{\ell(t)} w \, \mathrm{d}x = \tfrac{1}{60} k_* \Upsilon(\mathcal{K}) \ell^3(t). \tag{A5}$$

Differentiating with respect to time the above expression, after freezing the dependence of k_* and $\mathcal{K}$ on the front velocity v', yields

$$\dot{A}_f = \tfrac{1}{20} k_* \Upsilon(\mathcal{K}) \ell^2(t) \dot{\ell}(t). \tag{A6}$$

However, due to the fluid loss at the back end,

$$\dot{A}_f = -w_\infty v. \tag{A7}$$

Hence, from (A5) and (A7), we deduce that

$$\dot{\ell}(t) = -\epsilon\,(t)\, v, \quad \epsilon\,(t) = \frac{20 w_\infty}{\ell^2(t) k_* \Upsilon(\mathcal{K})}. \tag{A8}$$

Thus, the velocity v' of the separation front can be estimated as

$$v' = v + \dot{\ell}(t) = (1 - \epsilon\,(t))\, v. \tag{A9}$$

References

Ball, T.V. & Neufeld, J.A. 2018 Static and dynamic fluid-driven fracturing of adhered elastica. *Phys. Rev. Fluids* **3** (7), 074101.

Bunger, A.P. & Cruden, A.R. 2011 Modeling the growth of laccoliths and large mafic sills: role of magma body forces. *J. Geophys. Res.* **116**, B02203.

Chopin, J., Vella, D. & Boudaoud, A. 2008 The liquid blister test. *Proc. R. Soc.* A **464**, 2887–2906.

Dixit, H.N. & Homsy, G.M. 2013 The elastic Landau–Levich problem. *J. Fluid Mech.* **732**, 5–28.

Flitton, J.C. & King, J.R. 2004 Moving-boundary and fixed-domain problems for a sixth-order thin-film equation. *Eur. J. Appl. Maths* **15** (06), 713–754.

Giacomin, A.J., Cook, J.D., Johnson, L.M. & Mix, A.W. 2012 Flexible blade coating. *J. Coat. Technol. Res.* **9** (3), 269–277.

Hewitt, D.R., Chini, G.P. & Neufeld, J.A. 2018 The influence of a poroelastic till on rapid subglacial flooding and cavity formation. *J. Fluid Mech.* **855**, 1170–1207.

Hewitt, I.J., Balmforth, N.J. & De Bruyn, J.R. 2015 Elastic-plated gravity currents. *Eur. J. Appl. Maths* **26** (01), 1–31.

Hosoi, A.E. & Mahadevan, L. 2004 Peeling, healing, and bursting in a lubricated elastic sheet. *Phys. Rev. Lett.* **93** (13), 137802.

Hutchinson, J.W. & Suo, Z. 1991 Mixed mode cracking in layered materials. *Adv. Appl. Mech.* **29**, 63–191.

Jeffrey, R.G., *et al.* 2000 Hydraulic fracturing applied to inducing longwall coal mine goaf falls. In *4th North American Rock Mechanics Symposium*, pp. 423–430. American Rock Mechanics Association.

King, J. 1989 The isolation oxidation of silicon: the reaction-controlled case. *SIAM J. Appl. Maths* **49** (4), 1064–1080.

Landau, L.D. & Levich, B. 1942 Dragging of liquid by a moving plate. *Acta Physicochim. USSR* **7**, 42–54.

Landau, L.D. & Lifshitz, E.M. 1986 *Theory of Elasticity*, 3rd edn., Course of Theoretical Physics, vol. 7. Pergamon Press.

Lister, J.R., Peng, G.G. & Neufeld, J.A. 2013 Viscous control of peeling an elastic sheet by bending and pulling. *Phys. Rev. Lett.* **111** (15), 154501.

Lister, J.R., Skinner, D.J. & Large, T.M.J. 2019 Viscous control of shallow elastic fracture: peeling without precursors. *J. Fluid Mech.* **868**, 119–140.

https://doi.org/10.1017/jfm.2021.328 Published online by Cambridge University Press

MAJIDI, C. & ADAMS, G.G. 2009 A simplified formulation of adhesion problems with elastic plates. *Pro. R. Soc. Lond.* A **465** (2107), 2217–2230.

MICHAUT, C. 2011 Dynamics of magmatic intrusions in the upper crust: theory and applications to laccoliths on earth and the moon. *J. Geophys. Res.* **116**, B05205.

MURDOCH, L.C. 2002 Mechanical analysis of idealized shallow hydraulic fracture. *J. Geotech. Geoenviron. Engng* **128** (6), 488–495.

SEIWERT, J., QUÉRÉ, D. & CLANET, C. 2013 Flexible scraping of viscous fluids. *J. Fluid Mech.* **715**, 424–435.

TAYLER, A.B. & KING, J.R. 1987 Free boundaries in semi-conductor fabrication. In *Free Boundary Problems: Theory and Applications* (ed. K.H. Hoffman & J. Sprekels), Pitman Research Notes in Mathematics, vol. 1, pp. 243–259. Longman Scientific & Technical.

TAYLOR, G.I. 1962 On scraping viscous fluid from a plane surface. In *Miszellaneen der Angewandten Mechanik (Festschrift Walter Tollmien)* (ed. M. Schafer), pp. 313–315.

THOREY, C. & MICHAUT, C. 2016 Elastic-plated gravity currents with a temperature-dependent viscosity. *J. Fluid Mech.* **805**, 88–117.

TSAI, V.C. & RICE, J.R. 2012 Modeling turbulent hydraulic fracture near a free surface. *J. Appl. Mech.* **79** (3), 031003.

WANG, Z.-Q. & DETOURNAY, E. 2018 The tip region of a near-surface hydraulic fracture. *Trans. ASME J. Appl. Mech.* **85** (4), 041010.

WARBURTON, K.L.P., HEWITT, D.R. & NEUFELD, J.A. 2020 The elastic Landau–Levich problem on a slope. *J. Fluid Mech.* **883**, A40.

YOUNG, C. 1999 Controlled-foam injection for hard rock excavation. In *Rock Mechanics for Industry, Proceedings of 37th U.S. Rock Mechanics Symposium, Vail, Colorado*, Vol 1, pp. 115–122. Balkema.

https://doi.org/10.1017/jfm.2021.328 Published online by Cambridge University Press